analytical chemistry

pubs.acs.org/ac Article

In Situ Observation of mtDNA Damage during Hepatic Ischemia-Reperfusion

Wen Zhang,[#] Simin Bi,[#] Ping Li,[*] Jihong Liu, Chunmiao Zhou, Xin Wang, Wei Zhang, Hui Wang, and Bo Tang[*]

Cite This: *Anal. Chem.* 2021, 93, 5782−5788 Read Online

ACCESS | Metrics & More | Article Recommendations | Supporting Information

ABSTRACT: Hepatic ischemia-reperfusion (IR) injury is a severe pathophysiological event during liver surgery or transplantation and could lead to liver failure or even death. The energy supply of mitochondria plays an essential role in preventing IR injury. Mitochondrial DNA (mtDNA) is involved in maintaining the balance of energy by participating in an oxidative phosphorylation process. However, the exact relationship between IR and mtDNA remains unclear by reason of the lack of an accurate real-time analysis method. Herein, we fabricated a mitochondria-targeting fluorescent probe (mtDNA-BP) to explore mtDNA stability and supervise the changes in mtDNA in IR liver. By virtue of pyridinium electropositivity and suitable size, mtDNA-BP could accumulate in mitochondria and insert into the mtDNA groove, which made mtDNA-BP fluoresce strongly. This is attributed to the reduction of the intramolecular rotation energy loss that is restricted by DNA. By in situ fluorescence imaging, we observed in real time that mtDNA damage was aggravated by deteriorating IR injury, so the ROS-mtDNA-mediated IR damage signal pathway was speculated. Furthermore, on the basis of mtDNA-BP real-time response capability for mtDNA, we established a drug-screening method for inhibiting IR injury and found superior therapeutic performance of two potential drugs: pioglitazone and salidroside. This work contributes to our understanding of mtDNA-related disease and provides a new drug analysis method.

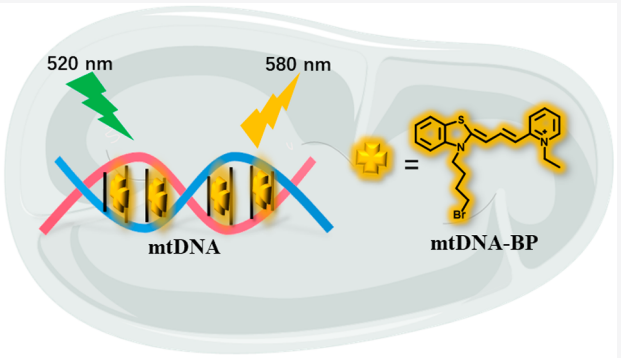

Ischemia-reperfusion (IR) is a routine operation, but a major obstacle in liver resection and transplantation surgery.[1,2] With the intent to resist hepatic IR injury, it ought to provide stronger support from mitochondria that generate ATP to maintain the internal stability of the organism and prevent disease.[3] Accordingly, the mitochondrial DNA (mtDNA) is involved in the oxidative phosphorylation process and closely related to ATP supply.[4] However, the exact relationship between IR and mtDNA remains unclear because of the lack of an accurate real-time analysis method. Therefore, to understand the obligatory role of mtDNA in liver IR injury, developing in situ real-time monitoring tools for mtDNA is extremely important.

Fluorescence microscopy is an authoritative tool to study concentration changes and location distributions of essential molecules.[5−8] This instrument contains many advantages including high resolution, simple operation, and in situ dynamic monitoring.[9−13] To make better use of fluorescence microscopy, many researchers have developed a variety of small-molecule fluorescent probes for tracking molecular events in cells and in vivo.[14−19] Although high-resolution imaging at the subcellular level was performed,[20−23] few probes can detect mtDNA located in the mitochondria of living cells. To reveal mtDNA-mediated IR damage, it is important to develop efficient probes and establish a real-time imaging method of the mtDNA level and distribution.

In this work, we constructed a small molecular mitochondrial-targeted probe mtDNA-BP (1-ethyl-2-{3-[3-(4-bromo)-butyl-2-benzothiazolinylidene]propenyl}pyridine bromide) for the detection of mtDNA (Figure 1). An appropriate size of mtDNA-BP was designed to embed in the DNA groove. Relying on the spatial constraints of DNA, the rotation of the pyridine ring was limited, and also the nonradiative transition of the excited state reduced, resulting in lighting up the DNA. Meanwhile, the unique electronegativity of the mitochondrial membrane could attract the pyridine cation to tread through the mitochondrial membrane and realize the mtDNA monitor. Utilizing mtDNA-BP, we traced the time-dependent damage of mtDNA during the IR process. Furthermore, a drug-screening method for protecting IR was devised by means of mtDNA-BP.

Received: December 13, 2020
Accepted: March 18, 2021
Published: March 30, 2021

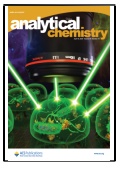

https://doi.org/10.1021/acs.analchem.0c05220
Anal. Chem. 2021, 93, 5782−5788

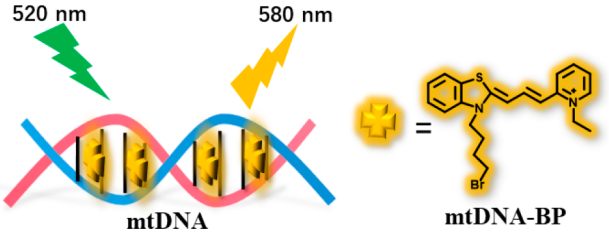

Figure 1. Design and luminescence mechanism of mtDNA-BP.

EXPERIMENTAL SECTION

Synthesis of 1-Ethyl-2-methylpyridine Bromide (1). The 2-methylpyridine (9.31 g, 0.1 mol) and ethyl bromide (10.89 g, 0.1 mol) were refluxed at 70 °C for 7 h and then allowed to cool down to room temperature; the resulting product was washed several times with ethyl ether and dried in vacuum to provide the crude product compound **1** (11.11 g, 0.091 mol, 90% crude yield). HRMS data, m/z calculated for $[C_8H_{12}N^+]$, 122.0964; found, 122.0956.

Synthesis of 1-Ethyl-2-[2-(phenylamino)ethenyl]-pyridine Bromide (2). Compound **1** (1.83 g, 15.0 mmol) and *N*,*N*′-diphenylformamidine (2.94 g, 15.0 mmol) were heated to 160 °C for 90 min. The resulting solid (compound **2**) was washed three times with ethyl ether and then dried in vacuum (0.78 g, 6.45 mmol, 48% yield). HRMS data, m/z calculated for $[C_{15}H_{17}N_2^+]$, 225.1386; found, 225.1393.

Synthesis of 1-(4-Bromo)-butyl-2-methylbenzothiazolium Bromide (3). The 2-methylbenzothiazole (1.49 g, 10.0 mmol) and 1,4-dibromo-butane (4.32 g, 20.0 mmol) were dissolved in 10 mL of toluene and heated to 110 °C for 17.5 h. After cooling, the solid was washed with ethyl ether and dried in vacuum to provide the crude product compound **3** (3.03 g, 8.3 mmol, 83% crude yield). HRMS data, m/z calculated for $[C_{12}H_{15}NSBr^+]$, 284.0109; found, 284.0115.

Synthesis of mtDNA-BP. The mtDNA-BP was synthesized by a simple and economical synthetic method and well-characterized [Figure 2, Figures S14−S19 (Supporting Information)]. The compounds **2** (0.34g, 1.5 mmol) and **3** (0.55g, 1.5 mmol) were dissolved in 15 mL 1:1 (v/v) CH_2Cl_2/CH_3OH soultion with 1.5 mL of $(Ac)_2O$ and 1.5 mL of $N(Et)_3$ and heated to 110 °C for 6.5 h. The black red solid (mtDNA-BP) was purified by silica gel column chromatography (CH_3OH/CH_2Cl_2, 1/20) and the product was collected (0.75 g, 1.8 mmol, 60% yield). HRMS data, m/z calculated for $[C_{21}H_{24}N_2SBr^+]$, 415.0838; found, 415.0824. ^{1}HNMR (400 MHz, $CDCl_3$): δ 8.54 (d, 1H), 7.81 (m, 2H), 7.57 (d, 1H), 7.42 (t, 1H), 7.25 (d, 1H), 7.06 (m, 2H), 6.29 (m, 2H), 5.24 (s, 1H), 4.49 (m, 2H), 4.04 (t, 2H), 3.59 (t, 2H), 1.93 (m, 2H), 1.49 (m, 5H). ^{13}CNMR (100 MHz, $CDCl_3$): δ 157.94, 157.85, 151.43, 141.93, 140.52, 139.03, 126.33, 123.44, 122.41, 121.14, 121.10, 120.99, 118.09, 117.96, 103.21, 62.67, 51.34, 43.85, 28.43, 24.96, 20.07.

Cytotoxicity Assay. We evaluated the cell viability by conventional MTT analysis. MTT reagent is 3-(4,5-dimethylthiazol-2-yl)-2,5-diphenyltetrazolium bromide (MTT).[24] We first grow HL-7702 cells at a density of 10^6 cells mL^{-1} into a 96-well plate of volume 200 μL $well^{-1}$. After 12 hours, numerous concentrations of mtDNA-BP (0, 1×10^{-9}, 1×10^{-8}, 1×10^{-7}, 1×10^{-6}, and 1×10^{-5} mol·L^{-1}) were added to the wells, and then the cells were incubated for an additional 24 h. Afterward, the MTT reagent (20 μL, 5 mg mL^{-1}) dissolved in DMSO was added to each well. After waiting for 4 h, we removed the MTT solution and then added 150 μL of DMSO to every well. Eventually, we used the Triturus microplate reader to measure the absorbance of the solution at 490 nm.

Models of Ischemia-Reperfusion in Cells and Mice. We constructed hepatic IR cell models by treating cells with oxygen and glucose deprivation/reperfusion. The ischemic state of hepatocytes was cultivated in DMEM without glucose and 0.5 mM deoxygenated sodium dithionite. Half an hour later, these cells were incubated with DMEM (high level of glucose) in a CO_2/O_2 (5/95) atmosphere as the state of reperfusion.[25]

Next, the IR mice model was established by 8-week-old wild-type Kunming female mice. We first used an intraperitoneal injection of 4% chloral hydrate to anesthetize the mice with a dosage of 3 mL kg^{-1}. Then we fixed the anesthetized mice onto the manipulator and cut open the abdomen of the mice to find the liver. Hepatic ischemia was achieved by gripping the vena and artery of the center and also the left lateral lobes of the liver with a microvessel clip, causing 70% liver anemia. And the reperfusion was performed by opening the vascular clamp. We have already obtained permission for the animal experiments from the Shandong Normal University authorities.

Extraction of Mitochondria and mtDNA. The mitochondria were isolated from liver tissue of normal and IR mice

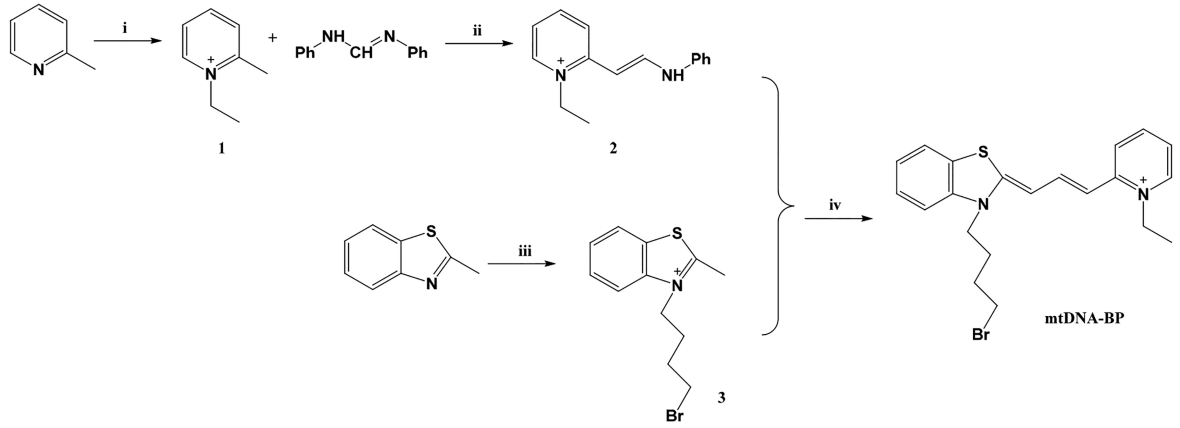

Figure 2. Synthesis of the probe mtDNA-BP. (i) Reflux, 7 h; (ii) 160 °C, 1.5 h; (iii) $Br(CH_2)_4Br$, toluene, 110 °C, 17.5 h; (iv) CH_2Cl_2, CH_3OH, $(Ac)_2O$, $N(Et)_3$, rt, 6.5 h.

https://doi.org/10.1021/acs.analchem.0c05220
Anal. Chem. 2021, 93, 5782−5788

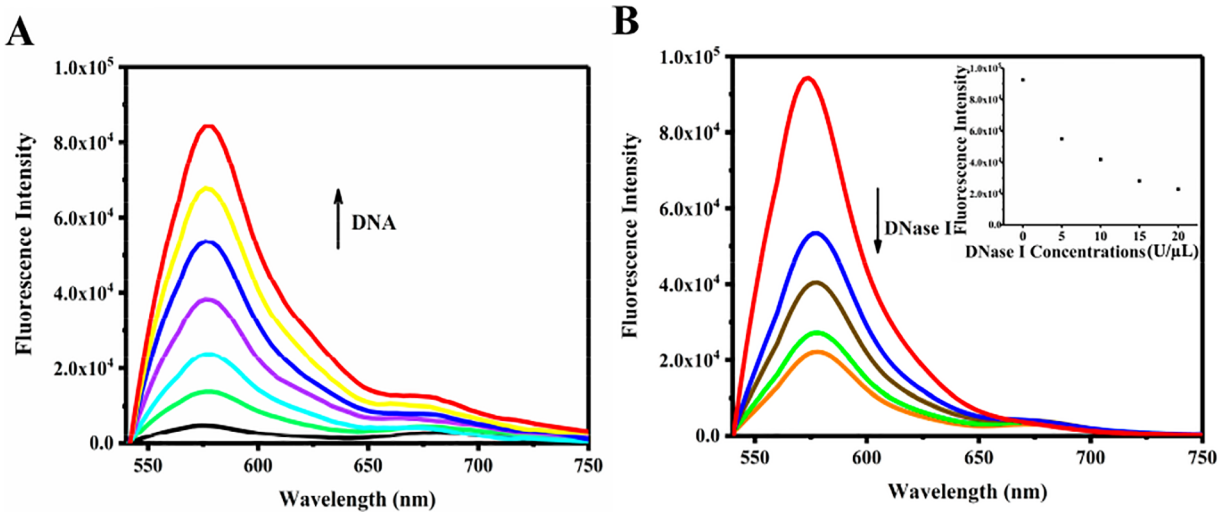

Figure 3. Fluorescent properties of mtDNA-BP for DNA detection. (A) Fluorescence responses of 5 μM mtDNA-BP toward the addition of DNA with various concentrations (0, 20, 40, 60, 80, 100, and 120 μg/mL). (B) Fluorescence spectra of 5 μM mtDNA-BP after the addition of 120 μg/mL DNA with different concentrations of DNase I (0, 5, 10, 15, and 20 U/mL). All spectra were acquired in Tris (pH 7.4) at λex/λem = 520/580 nm.

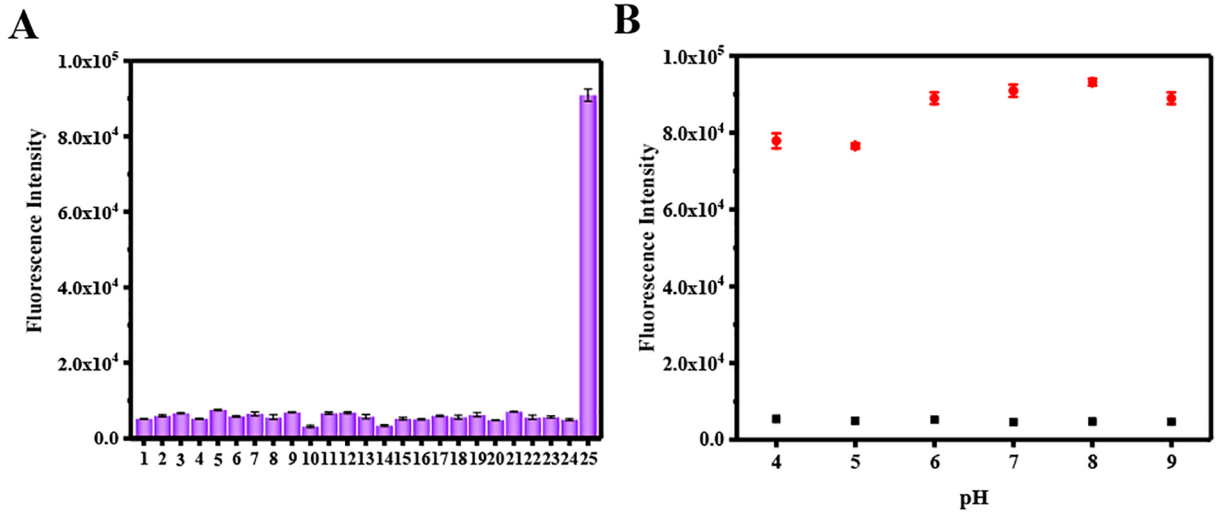

Figure 4. Fluorescence selectivity of mtDNA-BP for DNA. (A) 5 μM mtDNA-BP was treated with 1−25:10 mM K^+, 10 mM Na^+, 100 μM Cu^+, 100 μM Cu^{2+}, 100 μM Fe^{3+}, 100 μM Fe^{2+}, 1 mM Zn^{2+}, 1 mM Ca^{2+}, 100 μM Mn^{2+}, 10 μM $O_2^{\bullet -}$, 100 μM $^1O_2$, 100 μM $^\bullet$OH, 10 mM H_2O_2, 100 μM $ONOO^-$, 100 μM NO, 100 μM NaClO, 100 μM L-Tyr, 100 μM L-His, 100 μM Glc, 100 μM Vc, 100 μM Cys, 100 μM GSH, 10 mM ATP, 15 mM RNA, 120 μg/mL DNA. All spectra were acquired in Tris (pH 7.4) at λex/λem = 520/580 nm. (B) 5 μM mtDNA-BP was loaded with (black) and without (red) 120 μg/mL DNA at varying pH values (4.0, 5.0, 6.0, 7.0, 8.0, and 9.0).

employing a Tissue Mitochondria Isolation Kit (Beyotime Biotechnology Co., Ltd.) and mtDNA was isolated from liver tissue of mice using a mtDNA isolation kit consistent with the kit's instructions.

Fluorescence Imaging Experiments. The living cells were detached and reseeded onto 15 mL glass-bottom dishes 24 h before imaging. Next, we pretreated the cells with mtDNA-BP for 30 min, removed the medium, and then washed the cells with 500 μL of PBS three times. Fluorescence imaging of living cells was then executed. Mitochondrial localization imaging was performed utilizing confocal fluorescence microscopy with a green fluorescence channel (λ_{ex} = 514 nm and λ_{em} = 540−630 nm) and a red fluorescence channel (λ_{ex} = 633 nm and λ_{em} = 640−700 nm). For the data processing, the average fluorescence intensity of each image in every process was obtained by selecting the areas of interest. We repeated each experiment at least three times to get the same results.

Quantification of mtDNA Damage. We used the mtDNA long-range PCR to measure the level of mtDNA damage in IR-injured cells. The human mtDNA sequence-specific primers were utilized to amplify a 10 kilo base pair (10 kbp) fragment of mtDNA. The following primers were used to amplify a 10-kb fragment of mtDNA: sense primer 5′-TTTCATCATGCGGAGATGTTGGATGG-3′ and antisense primer 5′-TCTAAGCCTCCTTATTCGAGCCGA-3′.

Flow Cytometry. Hepatocytes seeded on 6-well plates were incubated continuously for 36−72 h at 37 °C in a CO_2 (5%) cell incubator with 2 mL of high-glucose DMEM per well. Before we performed the flow cytometry experiments, we washed pretreated hepatocytes with 2 mL of PBS and then treated them with 400 μL of 0.05% trypsin for 1 min. The

https://doi.org/10.1021/acs.analchem.0c05220
Anal. Chem. 2021, 93, 5782−5788

trypsin was discarded and 1 mL of high-glucose DMEM was added to each well. Subsequently, the hepatocytes were centrifuged for 5 min at 1000 rpm and the medium discarded. Then the hepatocytes were resuspended in 2 mL of PBS and once more centrifuged for 5 min at 1000 rpm. Afterward, every pellet was nurtured with Annexin V-FITC binding buffer (195 μL), Annexin V-FITC (5 μL), and propidium iodide (PI) (10 μL) in the dark at room temperature for 20 min. When the incubation operation was completed, the hepatocytes were centrifuged for 5 min at 1000 rpm and resuspended in PBS (200 μL). Lastly, the hepatocytes were subjected to flow cytometry. The fluorescence signals within the two channels of FITC and PI were surveyed for 5000 cells on an ImageStreamX Mark II flow cytometer (Merck). The data was analyzed by IDEAS software version 6.2.

RESULTS AND DISCUSSION

Properties of mtDNA-BP. We exploited the mtDNA-BP spectral property responding to DNA by using UV−vis and fluorescence spectra in a simulated physiological environment. As illustrated in Figure S1, upon addition of 120 μg/mL DNA, the maximum absorption wavelength appeared at 520 nm. Around the maximum fluorescence emission peak at 580 nm, the mtDNA-BP fluorescence intensity increased obviously with the addition of DNA while decreasing significantly with various DNase treatments (Figure 3). Furthermore, the fluorescence intensity enhanced linearly with the DNA concentrations rising (Figure S2). The linear range of DNA detection was 0−120 μg/mL and the limit of detection was 0.2331 μg/mL. These data prove that mtDNA-BP has a superior ability to detect DNA.

A high concentration of reactive oxygen species (ROS) and reactive nitrogen species exist in mitochondria, and there are amounts of metal ions in the path of mtDNA-BP entering mitochondria. All the disruptors may interfere with the fluorescence response of the probe, so the selectivity of mtDNA-BP should be investigated efficiently. Figure 4A shows that there were no significant fluorescence changes of mtDNA-BP toward intracellular active species except for DNA. It indicates that mtDNA-BP could detect DNA in cells exclusively. In addition, to further validate the mtDNA-BP specificity to DNA in a more realistic life environment, we performed a complete extraction of the mitochondria within the hepatocytes. In the mitochondrial internal fluid containing DNA, whether the mtDNA-BP is affected by other factors was investigated. As shown in Figure S3, the mtDNA-BP fluorescent in the authentic mitochondrial environment was not disturbed by ROS, metal ions, amino acids, and RNA. The coexistence interference experiment was consistent with the selectivity experiment in Figure 4A, further illustrating the distinctive response of the probe for DNA in a complex living environment. Besides, in view of the unbalanced distribution of $[H^+]$ in the subcellular region, the influence of pH fluctuations has been estimated. As shown in Figure 4B, the fluorescence signal of mtDNA-BP was varied imperceptibly in the physiological pH range 4.0−9.0. The experimental results show that mtDNA-BP has the potential to perform intracellular imaging without being disturbed by the intracellular microenvironment.

The faster the probe responds to the object, the easier it is to capture rapidly changing information about the active molecule. So, the DNA response rate of mtDNA-BP was explored. As shown in Figure S4, mtDNA-BP could recognize DNA transiently, which is beneficial for pick up the real-time information hinted at by DNA changes. Furthermore, the probe used for biological imaging should not add toxicity or side effects to the cells. Hence, the cytotoxicity assays were executed by MTT analysis (Figure S5). The IC_{50} of mtDNA-BP is 38.02 mM. It indicates that mtDNA-BP is a qualified imaging reagent with high velocity and safety.

Binding DNA Properties of mtDNA-BP. Studying the ability of mtDNA-BP to bind to DNA can provide a basis for their application in complex life units. Hence, we explored in detail the binding mode and ability of mtDNA-BP to DNA by SYBR Green I displacement assay.[26,27] SYBR Green I is a commercial DNA binding dye that indicates the degree of binding to DNA by changes in its fluorescence intensity. According to the Figure S6, when the SYBR Green I encountered the DNA, it exhibited intense fluorescence emission at 520 nm. Then the fluorescence intensity of SYBR Green I decreased with the addition of mtDNA-BP, and the fluorescence intensity decreased linearly with the increase of the probe concentrations. This indicated that SYBR Green I was extruded from the DNA groove by mtDNA-BP, and also suggested that the mtDNA-BP could embed in the DNA groove and had stronger binding ability to the DNA groove. In addition, we calculated the binding constants of mtDNA-BP to DNA based on the following equation (1)[28] and binding constant $K = 46773.51\ L{\cdot}mol^{-1}$ (Figure S7). Overall, the mtDNA-BP could be embedded in DNA grooves and have strong interactions with DNA.

$$\log[(F_0 - F)/F] = \log K + n \log[Q] \quad (1)$$

where F_0 and F are the fluorescence intensity without and with mtDNA-BP.

Mitochondrial Localization of mtDNA-BP. We exploited the distribution of mtDNA-BP in living cells.[29−31] Interestingly, mtDNA-BP prominently accumulated in mitochondria relying on the positive charge of the pyridine group. We employed the mitochondrial commercial dyes (MitoTracker Deep Red, Invitrogen, red channel) to co-stain with mtDNA-BP (green channel). As shown in Figure 5, all of the green fluorescence overlaid with the partly red color to exhibit yellow. Moreover, the distribution of green fluorescence was characterized by discrete points. This indicates that the probes could target specific regions within the mitochondria. Furthermore, we investigated whether mtDNA-BP could recognize mtDNA. Figure S8 showed that the fluorescence intensity of mtDNA-BP was significantly enhanced with the addition of mtDNA and the fluorescence intensity was reduced with Hind III (mtDNA digested enzyme) pretreated living cells. These data imply that mtDNA-BP could specifically image mtDNA in hepatic cells.

Real-Time Fluorescence Imaging of mtDNA-BP in IR Injury. Mitochondrial DNA plays a significant role in maintaining normal liver function by participating in the oxidative phosphorylation process for the supply of energy. The balance of the energy in the mitochondria is an important factor to resist IR damage. There seems to be a close link between mtDNA and IR injury. However, current research has not been able to determine the definite relationship. So, we tried to understand the communication between IR damage and mtDNA with the help of mtDNA-BP. The mtDNA fluctuations in the IR process were visualized in real time. As shown in Figure 6, with the time course of IR injury, the mtDNA-BP fluorescence intensity was gradually decreased for

https://doi.org/10.1021/acs.analchem.0c05220
Anal. Chem. 2021, 93, 5782−5788

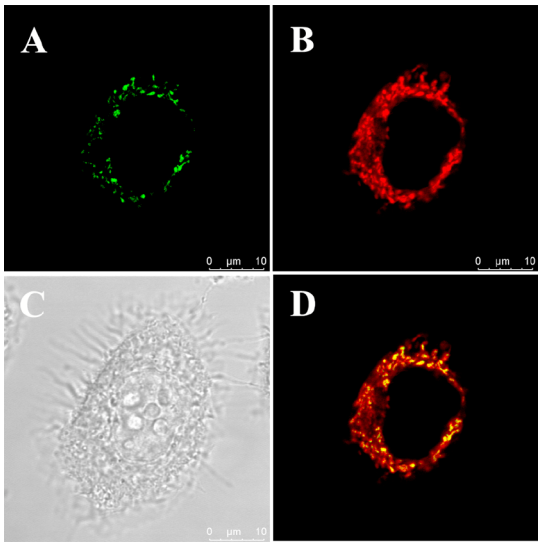

Figure 5. Mitochondrial colocalization experiment. Confocal fluorescence images of hepatocytes coincubated with 5 μM mtDNA-BP and 5 μM MitoTracker Red. (A) mtDNA-BP fluorescence was collected at 540−630 nm with 514 nm excitation. (B) MitoTracker Red fluorescence was collected at 660−730 nm with 633 nm excitation. (C) Bright-field imaging. (D) Merged image of A and B. Scale bar = 10 μm.

1 h. It showed mtDNA damage was aggravated by the deteriorating IR process and finally destroyed the mtDNA. To further verify the validity of the fluorescence imaging results, we performed a quantitative study of mtDNA based on a long patch PCR-based approach.[32,33] As shown in Figure S9, the amount of healthy mtDNA was significantly reduced in the IR group compared to the control group. And the degree of DNA damage increased with the duration of IR. These results demonstrate that IR injury caused the damage in mtDNA. The consistency of fluorescence imaging with PCR experimental results indicate that mtDNA-BP is a powerful tool for revealing the real-time relationship between IR and mtDNA.

Our previous real-time fluorescence imaging experiment found that superoxide and peroxynitrite anion were important regulatory factors in IR injury.[34,35] It can be seen that the abnormal change of ROS at the cellular level is an important factor for IR damage. Here, we further identified the changes in total ROS levels in IR mitochondria by employing the ROS assay kit. As shown in Figure S10, the stronger fluorescence was exhibited in the mitochondria of the IR group compared to that of the normal group, indicating that the total mitochondrial ROS was indeed abnormally elevated in IR. However, it is still not clear whether ROS also mediates mtDNA damage from IR. Hence, we explored the behavior of H_2O_2 to mtDNA via a simple extraction method of the liver. As shown in Figure S11, when the mitochondrial DNA was pretreated with 10 μM H_2O_2, the mtDNA-BP fluorescence intensity was reduced significantly. It suggested that overloaded ROS could mediate mtDNA damage, resulting in 8-hydroxydeoxyguanosine formation and mtDNA fragmentation, also causing the cross-linking of mtDNA to proteins.[36] Considering that the location of mtDNA is close to the respiratory chain complex produced by ROS in large quantities, and there is a lack of protective histone protein and some DNA repair activities in mitochondria, oxidative damage caused by ROS to mtDNA is more likely to occur.[37] And the ultimate fate of most IR cells was apoptosis and necrosis (Figure S12). The survival rate of IR injury cells was 66.45%, which was quite lower than the 87.54% survival rate of normal cells. This is consistent with the results of MTT analysis (Figure S13). We speculated on the signal pathway of ROS-mtDNA mediated IR injury, which provided a new idea about the IR injury therapeutic targets (Figure 7).

Figure 7. Signaling pathway of ROS-mtDNA-mediated IR injury.

Protective Effects of Drugs on IR Hepatocyte. On the basis of the experimental results we found above, the mtDNA might be implemented as a potential therapeutic evaluation target. Therefore, the drug-screening platform for inhibiting IR injury had been established based on the mtDNA real-time response capability of the probe. Promising drugs to treat IR injury were selected from the known literature.[38−46] As shown in Figure 8, precultured only with pioglitazone (100 μM) or salidroside (100 μM), IR hepatocytes still emitted bright fluorescence in accordance with the normal group. Obviously, these two potential drugs can protect mtDNA. To prove the validity of the probe-based screening method, we evaluated the therapeutic effect of selected drugs. We performed flow

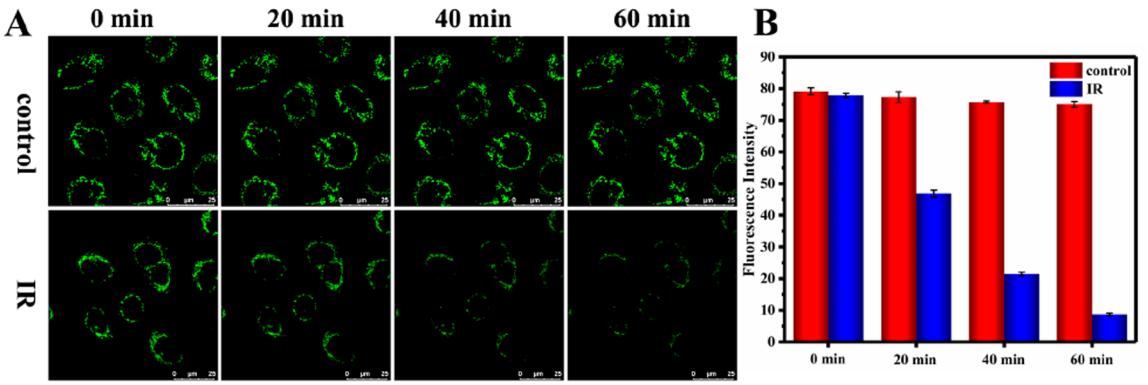

Figure 6. Time course of IR injury. (A) The hepatocytes incubated with 5 μM mtDNA-BP suffered ischemia for 20 min and then reperfusion for 40 min. (B) Average fluorescence intensity output of A. The fluorescence images were collected at 540−630 nm with an excitation wavelength of 514 nm. Scale bar = 25 μm.

https://doi.org/10.1021/acs.analchem.0c05220
Anal. Chem. 2021, 93, 5782−5788

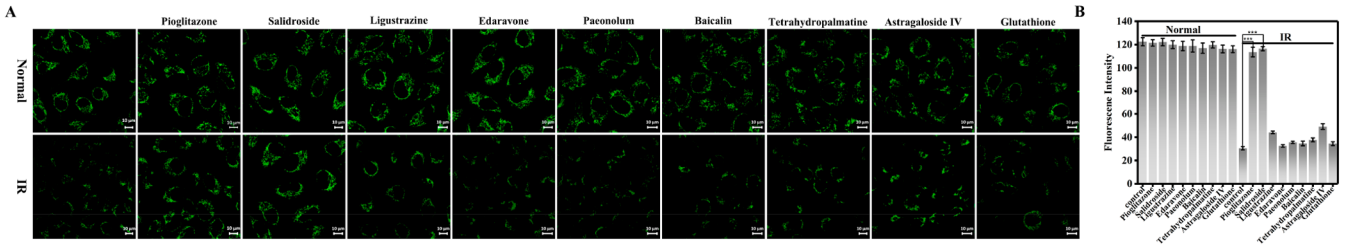

Figure 8. Protective effects of drugs on IR hepatocyte. (A) 5 μM mtDNA-BP-labeled HL-7702 cells were preincubated with the drugs for only 24 h; the IR group suffered ischemia for 30 min and reperfusion for 30 min. (B) Average fluorescence intensity output of A. Fluorescence images were collected at 540−630 nm with an excitation wavelength of 514 nm. Scale bar = 10 μm, P = 0.001.

cytometry analysis to estimate the survival rate of liver cells (Figure S12). Compared to the IR group (66.45%), the survival rate of the two drugs preconditioning groups were significantly higher (pioglitazone 90.20% and salidroside 86.24%). These results clearly demonstrate the rationality and reliability of the drug platform design based on mtDNA-BP, and the pioglitazone and salidroside show strong protective effects for the mtDNA to resist IR injury.

CONCLUSION

In summary, we have developed a DNA-targeted fluorescence probe mtDNA-BP for in situ real-time detections of mtDNA. The mtDNA-BP was constructed with a proper molecular size and pyridine cation displaying turn-on fluorescent responses with mtDNA. This probe exhibited a suitable combination of high specificity, exclusive mtDNA targeting, and fast response. With facilitation of mtDNA-BP, we successfully monitored mtDNA levels in real time in hepatic IR injury and disclosed the ROS-mtDNA-mediated IR injury signaling pathway. We also built the drug-screening method for inhibiting IR injury by relying on mtDNA-BP, and two potential effective drugs were screened out. Our probe can be expanded to mtDNA-related disease and be used to support new drug discovery for those diseases associated with mtDNA disharmony.

ASSOCIATED CONTENT

Supporting Information

The Supporting Information is available free of charge at https://pubs.acs.org/doi/10.1021/acs.analchem.0c05220.

Additional experimental data, including experimental details, photophysical properties, cytotoxicity, and characterization (PDF)

AUTHOR INFORMATION

Corresponding Authors

Bo Tang − *College of Chemistry, Chemical Engineering and Materials Science, Key Laboratory of Molecular and Nano Probes, Ministry of Education, Collaborative Innovation Center of Functionalized Probes for Chemical Imaging in Universities of Shandong, Institutes of Biomedical Sciences, Shandong Normal University, Jinan 250014, People's Republic of China;* orcid.org/0000-0002-8712-7025; Email: tangb@sdnu.edu.cn

Ping Li − *College of Chemistry, Chemical Engineering and Materials Science, Key Laboratory of Molecular and Nano Probes, Ministry of Education, Collaborative Innovation Center of Functionalized Probes for Chemical Imaging in Universities of Shandong, Institutes of Biomedical Sciences, Shandong Normal University, Jinan 250014, People's Republic of China;* orcid.org/0000-0002-2356-0962; Email: lip@sdnu.edu.cn

Authors

Wen Zhang − *College of Chemistry, Chemical Engineering and Materials Science, Key Laboratory of Molecular and Nano Probes, Ministry of Education, Collaborative Innovation Center of Functionalized Probes for Chemical Imaging in Universities of Shandong, Institutes of Biomedical Sciences, Shandong Normal University, Jinan 250014, People's Republic of China*

Simin Bi − *College of Chemistry, Chemical Engineering and Materials Science, Key Laboratory of Molecular and Nano Probes, Ministry of Education, Collaborative Innovation Center of Functionalized Probes for Chemical Imaging in Universities of Shandong, Institutes of Biomedical Sciences, Shandong Normal University, Jinan 250014, People's Republic of China*

Jihong Liu − *College of Chemistry, Chemical Engineering and Materials Science, Key Laboratory of Molecular and Nano Probes, Ministry of Education, Collaborative Innovation Center of Functionalized Probes for Chemical Imaging in Universities of Shandong, Institutes of Biomedical Sciences, Shandong Normal University, Jinan 250014, People's Republic of China;* orcid.org/0000-0003-3306-7802

Chunmiao Zhou − *College of Chemistry, Chemical Engineering and Materials Science, Key Laboratory of Molecular and Nano Probes, Ministry of Education, Collaborative Innovation Center of Functionalized Probes for Chemical Imaging in Universities of Shandong, Institutes of Biomedical Sciences, Shandong Normal University, Jinan 250014, People's Republic of China*

Xin Wang − *College of Chemistry, Chemical Engineering and Materials Science, Key Laboratory of Molecular and Nano Probes, Ministry of Education, Collaborative Innovation Center of Functionalized Probes for Chemical Imaging in Universities of Shandong, Institutes of Biomedical Sciences, Shandong Normal University, Jinan 250014, People's Republic of China*

Wei Zhang − *College of Chemistry, Chemical Engineering and Materials Science, Key Laboratory of Molecular and Nano Probes, Ministry of Education, Collaborative Innovation Center of Functionalized Probes for Chemical Imaging in Universities of Shandong, Institutes of Biomedical Sciences, Shandong Normal University, Jinan 250014, People's Republic of China*

Hui Wang − *College of Chemistry, Chemical Engineering and Materials Science, Key Laboratory of Molecular and Nano Probes, Ministry of Education, Collaborative Innovation Center of Functionalized Probes for Chemical Imaging in*

https://doi.org/10.1021/acs.analchem.0c05220
Anal. Chem. 2021, 93, 5782−5788

Universities of Shandong, Institutes of Biomedical Sciences, Shandong Normal University, Jinan 250014, People's Republic of China

Complete contact information is available at: https://pubs.acs.org/10.1021/acs.analchem.0c05220

Author Contributions

[#]W.Z. and S.B. contributed equally.

Notes

The authors declare no competing financial interest.

■ ACKNOWLEDGMENTS

This work was supported by the National Natural Science Foundation of China (21535004, 91753111, 21675105, 22077075, and 21927811), the Key Research and Development Program of Shandong Province (2018YFJH0502), and National Major Scientific and Technological Special Project for "Significant New Drugs Development" (2017ZX09301030004).

■ REFERENCES

(1) Cannistra, M.; Ruggiero, M.; Zullo, A.; Gallelli, G.; Serafini, S.; Maria, M.; Naso, A.; Grande, R.; Serra, R.; Nardo, B. *Int. J. Surg.* **2016**, *33* (1), S57−S70.
(2) Nardo, B.; Ercolani, G.; Montalti, R.; Bertelli, R.; Gardini, A.; Beltempo, P.; Puviani, L.; Pacile, V.; Vivarelli, M.; Cavallari, A. *J. Am. Coll. Surg.* **2005**, *201* (5), 671−679.
(3) Green, D. R.; Reed, J. C. *Science* **1998**, *281* (5381), 1309−1312.
(4) Dhalla, N. S.; Panagia, V.; Singal, P. K.; Makino, N.; Cardiology, C. *J. Mol. Cell. Cardiol.* **1988**, *20* (2), 3−13.
(5) Wu, X.; Sun, X.; Guo, Z.; Tang, J.; Shen, Y.; James, T. D.; Tian, H.; Zhu, W. *J. Am. Chem. Soc.* **2014**, *136* (9), 3579−3588.
(6) Rudd, A. K.; Mittal, N.; Lim, E. W.; Metallo, C. M.; Devaraj, N. K. *J. Am. Chem. Soc.* **2020**, *142* (42), 17887−17891.
(7) Morstein, J.; Hofler, D.; Ueno, K.; Jurss, J. W.; Walvoord, R. R.; Bruemmer, K. J.; Rezgui, S. P.; Brewer, T. F.; Saitoe, M.; Michel, B. W.; Chang, C. J. *J. Am. Chem. Soc.* **2020**, *142* (37), 15917−15930.
(8) Nguyen, V. N.; Yim, Y.; Kim, S.; Ryu, B.; Swamy, K. M. K.; Kim, G.; Kwon, N.; Kim, C. Y.; Park, S.; Yoon, J. *Angew. Chem., Int. Ed.* **2020**, *59* (23), 8957−8962.
(9) Murfin, L. C.; Weber, M.; Park, S. J.; Kim, W. T.; Lopez-Alled, C. M.; McMullin, C. L.; Pradaux-Caggiano, F.; Lyall, C. L.; Kociok-Kohn, G.; Wenk, J.; Bull, S. D.; Yoon, J.; Kim, H. M.; James, T. D.; Lewis, S. E. *J. Am. Chem. Soc.* **2019**, *141* (49), 19389−19396.
(10) Zhang, J.; Fu, Y.; Han, H. H.; Zang, Y.; Li, J.; He, X. P.; Feringa, B. L.; Tian, H. *Nat. Commun.* **2017**, *8* (1), 987.
(11) Wu, S.; Ma, C.; Gao, Y.; Su, Y.; Xia, Q.; Chen, Z.; Zhu, J. J. *Anal. Chem.* **2020**, *92* (14), 9940−9947.
(12) Yang, S.; Jiang, J.; Zhou, A.; Zhou, Y.; Ye, W.; Cao, D. S.; Yang, R. *Anal. Chem.* **2020**, *92* (10), 7194−7199.
(13) Takahashi, S.; Kagami, Y.; Hanaoka, K.; Terai, T.; Komatsu, T.; Ueno, T.; Uchiyama, M.; Koyama-Honda, I.; Mizushima, N.; Taguchi, T.; Arai, H.; Nagano, T.; Urano, Y. *J. Am. Chem. Soc.* **2018**, *140* (18), 5925−5933.
(14) Ge, J.; Hu, Y.; Deng, R.; Li, Z.; Zhang, K.; Shi, M.; Yang, D.; Cai, R.; Tan, W. *Anal. Chem.* **2020**, *92* (19), 13588−13594.
(15) Xiong, M.; Yang, Z.; Lake, R. J.; Li, J.; Hong, S.; Fan, H.; Zhang, X. B.; Lu, Y. *Angew. Chem., Int. Ed.* **2020**, *59* (5), 1891−1896.
(16) Yan, X.; Xia, C.; Chen, B.; Li, Y. F.; Gao, P. F.; Huang, C. Z. *Anal. Chem.* **2020**, *92* (2), 2130−2135.
(17) Yang, M.; Huang, J.; Fan, J.; Du, J.; Pu, K.; Peng, X. *Chem. Soc. Rev.* **2020**, *49* (19), 6800−6815.
(18) Liu, Y.; Wolstenholme, C. H.; Carter, G. C.; Liu, H.; Hu, H.; Grainger, L. S.; Miao, K.; Fares, M.; Hoelzel, C. A.; Yennawar, H. P.; Ning, G.; Du, M.; Bai, L.; Li, X.; Zhang, X. *J. Am. Chem. Soc.* **2018**, *140* (24), 7381−7384.
(19) He, S.; Song, B.; Li, D.; Zhu, C.; Qi, W.; Wen, Y.; Wang, L.; Song, S.; Fang, H.; Fan, C. *Adv. Funct. Mater.* **2010**, *20* (3), 453−459.
(20) Yu, C. Y.; Xu, H.; Ji, S.; Kwok, R. T.; Lam, J. W.; Li, X.; Krishnan, S.; Ding, D.; Tang, B. Z. *Adv. Mater.* **2017**, *29* (15), 1606167.
(21) He, L.; Yang, X.; Xu, K.; Lin, W. *Chem. Commun.* **2017**, *53* (29), 4080−4083.
(22) Wu, Z.; Liu, M.; Liu, Z.; Tian, Y. *J. Am. Chem. Soc.* **2020**, *142* (16), 7532−7541.
(23) Li, H.; Shi, W.; Li, X.; Hu, Y.; Fang, Y.; Ma, H. *J. Am. Chem. Soc.* **2019**, *141* (45), 18301−18307.
(24) Gerlier, D.; Thomasset, N. *J. Immunol. Methods* **1986**, *94* (1−2), 57−63.
(25) Liu, R.; Zhang, L.; Lan, X.; Li, L.; Zhang, T. T.; Sun, J. H.; Du, G. H. *Neuroscience* **2011**, *176*, 408−419.
(26) McKeague, M.; Velu, R.; Hill, K.; Bardóczy, V.; Mészáros, T.; DeRosa, M. *Toxins* **2014**, *6*, 2435−2452.
(27) Dragan, A. I.; Pavlovic, R.; McGivney, J. B.; Casas-Finet, J. R.; Bishop, E. S.; Strouse, R. J.; Schenerman, M. A.; Geddes, C. D. *J. Fluoresc.* **2012**, *22*, 1189−1199.
(28) Ahmad, B.; Parveen, S.; Khan, R. H. *Biomacromolecules* **2006**, *7* (4), 1350−1356.
(29) Zou, X.; Shi, Y.; Zhu, R.; Han, J.; Han, S. *Anal. Chem.* **2019**, *91* (24), 15899−15907.
(30) Feng, B.; Wang, K.; Yang, Y.; Wang, G.; Zhang, H.; Liu, Y.; Jiang, K. *Chem. Sci.* **2019**, *10* (44), 10373−10380.
(31) Feng, B.; Wang, K.; Liu, J.; Mao, G.; Cui, J.; Xuan, X.; Jiang, K.; Zhang, H. *Anal. Chem.* **2019**, *91* (21), 13962−13969.
(32) Das, B. B.; Dexheimer, T. S.; Maddali, K.; Pommier, Y. *Proc. Natl. Acad. Sci. U. S. A.* **2010**, *107* (46), 19790−19795.
(33) Ghosh, A.; Bhattacharjee, S.; Chowdhuri, S. P.; Mallick, A.; Rehman, I.; Basu, S.; Das, B. B. *Sci. Adv.* **2019**, *5* (11), eaax9778.
(34) Zhang, W.; Liu, J.; Li, P.; Wang, X.; Bi, S.; Zhang, J.; Zhang, W.; Wang, H.; Tang, B. *Biomaterials* **2019**, *225*, 119499.
(35) Zhang, W.; Li, P.; Yang, F.; Hu, X.; Sun, C.; Zhang, W.; Chen, D.; Tang, B. *J. Am. Chem. Soc.* **2013**, *135* (40), 14956−14959.
(36) Richter, C. *Int. J. Biochem. Cell Biol.* **1995**, *27* (7), 647−653.
(37) Beckman, K. B.; Ames, B. N. *Mutat. Res., Fundam. Mol. Mech. Mutagen.* **1999**, *424* (1−2), 51−58.
(38) Elshazly, S.; Soliman, E. *Toxicol. Appl. Pharmacol.* **2019**, *362*, 86−94.
(39) Sun, L.; Isaak, C. K.; Zhou, Y.; Petkau, J. C.; O, K.; Liu, Y.; Siow, Y. L. *Life Sci.* **2012**, *91* (5−6), 151−158.
(40) Lv, L.; Jiang, S. S.; Xu, J.; Gong, J. B.; Cheng, Y. *Clin. Exp. Pharmacol. Physiol.* **2012**, *39* (1), 20−27.
(41) Reyes, Y. A.; Shimoyama, T.; Akamatsu, H.; Sunamori, M. *Eur. J. Cardiothorac. Surg.* **2006**, *29* (3), 304−311.
(42) Mohamed, M. Z.; Morsy, M. A.; Mohamed, H. H.; Hafez, H. M. *Andrologia* **2020**, *52* (6), No. e13599.
(43) Lin, M.; Li, L.; Li, L.; Pokhrel, G.; Qi, G.; Rong, R.; Zhu, T. *BMC Complementary Altern. Med.* **2014**, *14* (1), 19.
(44) Yu, Q.; Wu, L.; Liu, T.; Li, S.; Feng, J.; Mao, Y.; Fan, X.; Guo, C.; Wu, J. *Int. Immunopharmacol.* **2019**, *70*, 435−445.
(45) Gui, D.; Huang, J.; Liu, W.; Guo, Y.; Xiao, W.; Wang, N. *Apoptosis* **2013**, *18* (4), 409−422.
(46) Qi, X.; Ng, K. T.; Lian, Q.; Li, C. X.; Geng, W.; Ling, C. C.; Yeung, W. H.; Ma, Y. Y.; Liu, X. B.; Liu, H.; Liu, J.; Yang, X. X.; Lo, C. M.; Man, K. *Theranostics* **2018**, *8* (1), 212−222.